Finite Spot Effects on Radiation Pressure Acceleration from Intense High-Contrast Laser Interactions with Thin Targets

F. Dollar,[1] C. Zulick,[1] A. G. R. Thomas,[1] V. Chvykov,[1] J. Davis,[2] G. Kalinchenko,[1] T. Matsuoka,[1] C. McGuffey,[1] G. M. Petrov,[2] L. Willingale,[1] V. Yanovsky,[1] A. Maksimchuk,[1] and K. Krushelnick[1]

[1]*Center for Ultrafast Optical Science, University of Michigan, Ann Arbor, Michigan 48109-2099, USA*
[2]*Plasma Physics Division, Naval Research Laboratory, Washington, D.C. 20375, USA*

(Received 7 January 2012; published 25 April 2012)

Short pulse laser interactions at intensities of 2×10^{21} W cm^{-2} with ultrahigh contrast (10^{-15}) on submicrometer silicon nitride foils were studied experimentally by using linear and circular polarizations at normal incidence. It was observed that, as the target decreases in thickness, electron heating by the laser begins to occur for circular polarization leading to target normal sheath acceleration of contaminant ions, while at thicker targets no acceleration or electron heating is observed. For linear polarization, all targets showed exponential energy spreads with similar electron temperatures. Particle-in-cell simulations demonstrate that the heating is due to the rapid deformation of the target that occurs early in the interaction. These experiments demonstrate that finite spot size effects can severely restrict the regime suitable for radiation pressure acceleration.

DOI: 10.1103/PhysRevLett.108.175005 PACS numbers: 52.38.Kd, 41.75.Jv, 52.50.Jm, 52.70.Nc

Some of the most promising applications of laser driven ion accelerators, such as ion therapy [1–4], rely on proton or ion beams accelerated to several hundreds of MeV per nucleon with a narrow energy spread. Previous studies have focused on the target normal sheath acceleration (TNSA) [5] mechanism, in which suprathermal electrons from the laser plasma interaction form a Debye sheath on the surface of a foil target. This sheath first ionizes and then accelerates the constituent protons and light ions of contaminants that naturally adhere to the target. TNSA has demonstrated proton beams with energies >60 MeV, yet with large energy spreads [6]. Several groups have demonstrated control over the proton energy spread by using energy selection [7], complex target preparation [8], and optical density shaping [9] and by driving ion soliton waves [10]. Several alternate schemes for utilizing ultrashort pulse lasers (pulse length $\approx$ 30 fs) have been proposed, including the breakout afterburner [11], directed Coulomb explosion [12], and the light-sail regime of radiation pressure acceleration (RPA) [13]. Recent experimental work investigating RPA has been performed, with either longer pulse durations and lower densities [14] or moderate intensities with high density, thin foils [15].

In RPA, circular polarization may inhibit the absorption of laser energy into thermal electrons, since $\mathbf{j} \times \mathbf{B}$ heating is absent, and consequently TNSA is suppressed. Momentum is imparted by the laser to the target material, either by the laser acting as a piston on a semi-infinite target (hole boring) [16] or by the laser accelerating the plasma as an accelerating mirror (light sail). In light-sail RPA, the entire focal volume is accelerated to the same momentum, producing narrow energy spread ions. In this model, ion energies are optimized when the foil thickness is $L \approx \frac{a_0}{\pi} \frac{n_{\mathrm{crit}}}{n_e} \lambda$, where a_0 is the normalized field strength, λ is the laser wavelength, and $\frac{n_{\mathrm{crit}}}{n_e}$ is the ratio of critical density to electron density. For $a_0 = 20$ at solid density the optimal thickness is calculated to be 15 nm [17]. However, many simulations have been performed in 1D, where no transverse effects exist. Those performed in 2D use parameters that minimize transverse spatial gradients [13,17,18].

In the RPA mechanism, suppression of electron heating will result in efficient energy transfer to the target ions. In this Letter, we show that for current ultrashort pulse laser systems ($E_p < 10J$) RPA is not practically attainable, since, as the target thickness decreases, electron heating occurs rather than RPA even for circular polarization. This results in proton and carbon beams with exponential energy distributions similar to linear polarization under identical conditions. Particle-in-cell simulations of the interaction demonstrate that rapid deformation of the thin target such that the laser field is not perpendicular to the surface normal results in efficient electron heating via a Brunel-like mechanism. For thicker targets where RPA is ineffective, target deformation is minimal within the pulse duration, resulting in no TNSA with the circular polarized pulse, consistent with our experimental results.

The experiments were performed by using the HERCULES laser facility at University of Michigan, a Ti:sapphire system ($\lambda = 800$ nm) producing laser pulses with $\tau = 40$ fs duration full width at half maximum (FWHM) and an amplified spontaneous emission intensity contrast of 10^{-11} [19]. Prior to the experimental chamber, mirrors in a secondary chamber focus the amplified pulse onto a pair of antireflection coated BK7 glass substrates that act as plasma mirrors. Each plasma mirror reflects <0.15% of S polarized light at 810 nm while possessing a measured reflectivity of 65%–70% at high intensity,

producing a nanosecond-level amplified spontaneous emission contrast of $<10^{-15}$. This contrast improvement should prevent preplasma formation until 1 ps before the main pulse interaction, so that the density profiles remain extremely sharp. After the plasma mirrors, a mica $\frac{\lambda}{4}$ wave plate enables changes the polarization (between linear and circular). Beam profile monitors recorded the near and far field patterns of the beam after the wave plate to verify focal spot quality and to confirm that the wave plate did not noticeably increase the pulse length.

In this experiment, the laser delivered 1.5 ($\pm$ 0.2) J to the target with 55% of the energy in a 1.2 μm FWHM focal spot via an $f/1$ off-axis parabolic mirror. This results in an on-target intensity of 2×10^{21} W cm^{-2} ($a_0 = 30$). A near diffraction limited spot size with a Strehl ratio of 0.6–0.9 was attained by using a deformable mirror (Xinetics) and a Shock-Hartmann wave front sensor, which are used to correct aberrations predominantly from the off-axis parabolic mirror.

The targets used in the experiment were freestanding silicon nitride membranes with thicknesses of 30–100 nm and 1 μm Mylar ($C_{10}H_8O_4$) foils. The targets were positioned at the laser focus with an accuracy of ± 2 μm (half of the Rayleigh length) at normal incidence. The experiment was performed with a linearly polarized beam and with a right-hand circular polarized beam that possessed the same focal quality albeit with $\sim$10% less total energy.

A Thomson parabola ion spectrometer (TP) in the rear target normal direction and a magnetic electron spectrometer 8° off target normal were the primary diagnostics for the measurements of ion energy spectra and electron energy spectra, respectively. In the TP, magnetic fields disperse by momenta, while an electric field provided a separation of the ion traces based on the charge to mass ratio of the ion species. The solid angle subtended by the TP is 9.6×10^{-8} sr. A microchannel plate detector [20] in the TP and a Lanex scintillating screen in the magnetic electron spectrometer allowed for real-time data acquisition. CR-39 track detectors with stacked filters were also used for absolute ion energy measurements. A *p-i-n* diode with a 25 μm Be filter and a dipole magnet in front measured x-ray emission above 2 keV from the interaction region on the front side of the target.

With linear polarization, all targets produced an exponential energy distribution for both proton and carbon beams. For 30 nm SiN, linear polarization produced protons with an average maximum energy of $\approx$ 13 MeV [Fig. 1(c)]. Several shots were taken for each condition. The smaller dispersion and higher noise in the spectra at higher energies increase the error bars for these thinnest targets. In several shots the spectra displayed some modulated structure. This is consistent with experiments performed previously [9]. The average maximum energy of the protons and carbon ions increases slightly as target thickness is decreased [Fig. 1(c)].

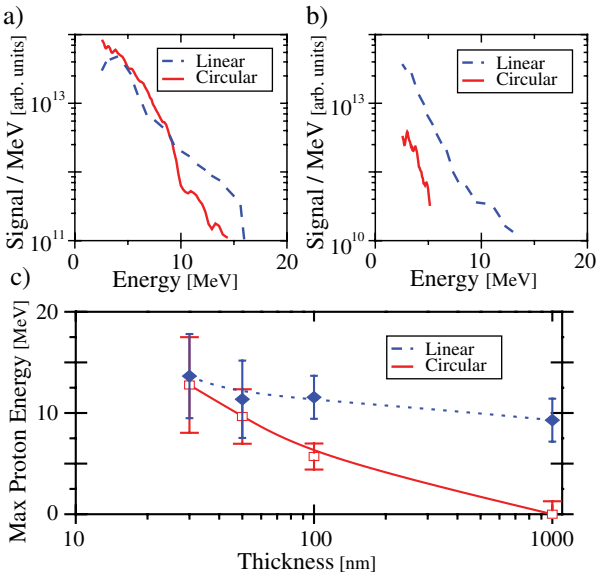

FIG. 1 (color online). Proton energy spectra for both right-hand circular and linearly polarized laser pulse interactions for (a) 30 and (b) 100 nm thickness SiN targets. Maximum proton energy vs target thickness is also shown (c) with lines shown as a visual aid only.

When the quarter wave plate was inserted (i.e., circular polarization), the maximum proton energy was below the spectral range of the TP for the case of the 1 μm Mylar targets. There was also no detectable electron signal. For the SiN targets, the proton maximum energies were low for the 100 nm target and then subsequently increased rapidly as the thickness decreased. For 100 nm targets, the maximum energy was 6 MeV, which increased to 12 MeV at 30 nm [Fig. 1(c)]. The energy spectra were exponential [Fig. 1(a)]. The electron spectrometer also showed an increase of maximum electron energy for decreasing thickness, such that for the 30 nm target thickness the spectra matched that of the linear case but was substantially weaker for the 100 nm case (Fig. 2). The x-ray diode showed an increase in signal for both linear and circular polarizations as the target thickness was decreased below 100 nm.

At energies beyond the end of the exponential tail of the energy spectra in both polarizations for the 30 nm targets, a small signal was also observed at relatively high energies in the carbon spectra [Figs. 3(a) and 3(b)]. The quasimonoenergetic peak was observed in the C_6^+ ion spectra that corresponded to energies between 3 and 12 MeV per nucleon. This peak had an energy spread of $\approx$ 66%, with the maximum energy for the circular case $\approx$ 2 MeV per nucleon higher than that of the linear case. Note that the dispersion was rather poor at these energies in the TP such that the error is $\approx$ 1 MeV per nucleon. It is also possible that this is due to fully ionized bulk target ions, as they possess an indistinguishable charge to mass ratio; however, due to the prominence of the C_5^+ ions compared to the Si

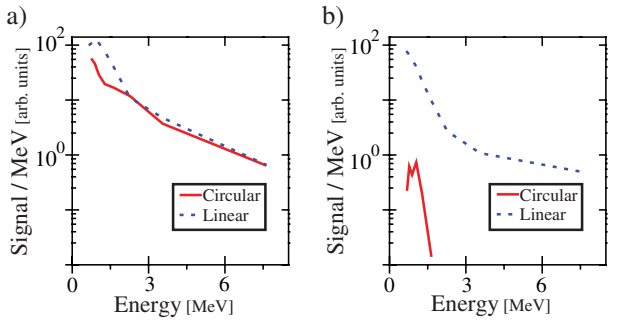

FIG. 2 (color online). Electron energy spectra for right-hand circular (solid line) and linear (dashed line) polarized laser pulse interaction for (a) 30 and (b) 100 nm SiN targets.

and N ions, it is more likely that it is due to C_6^+ ions. It is possible that such a signal exists for the protons as well, but the response of the microchannel plate to protons is weaker than that to carbon ions, and there consequently was not a sufficiently strong signal on the CR-39 and the microchannel plate to distinguish from background.

The increased electron energy indicates that, rather than achieving RPA, we are predominantly coupling laser energy to electron heating. It is unlikely that the target expanded to a subcritical density ($< 10^{21}$ cm^{-3}) by prepulse for the circular case, as this would suggest far more expansion when compared to the linear case, leading to a drop in maximum proton energy [21] which was not observed experimentally. To determine the source of the electron heating, simulations using the 2D3P particle-in-cell code OSIRIS [22] were performed. A fully ionized carbon target ($n_e = 500 n_{\mathrm{crit}}$) with 6 nm proton layers ($n_e = 100 n_{\mathrm{crit}}$) on the front and rear surfaces was used to match the experimental conditions of contaminants on a

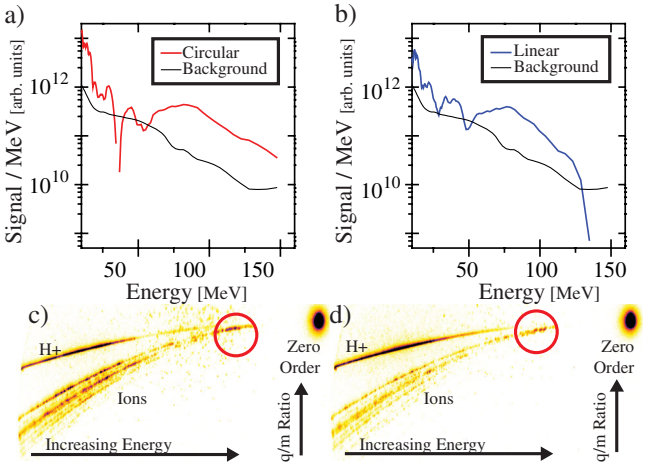

FIG. 3 (color online). C_6^+ energy spectra for (a) right-hand circular and (b) linear polarized laser pulse interaction for 30 nm SiN targets. Detector background levels are shown for comparison. Raw spectra are shown for (c) circular and (d) linear polarization, with the high energy carbon peak denoted by the red circle.

thin foil, in contrast to many simulations performed prior. The input polarization and the target thickness were also varied. The target thicknesses used were 24 (thin) and 96 nm (thick) to give a total target thickness of 36 and 108 nm, respectively, with a transverse dimension of 14 μm. The incident pulse had a pulse length of 40 fs and a field strength parameter of $a_0 = 30$ focused to a 1.1 μm FWHM Gaussian spot. The cell size was 2.88 nm in both directions with at least 32 particles per cell (256 particles per cell for the proton layer).

For thin targets, initially the target focal area is accelerated forward by RPA with minimal electron heating, but as the target becomes rapidly deformed, the electrons begin to be heated efficiently via direct laser acceleration [23] and Brunel heating [24], because the target surface normal is no longer perpendicular to the laser field. For the circular heating case, we can observe this heating due to surface deformation by considering the variance of the transverse electron momenta and the mean target displacement along the laser axis. Plotting these values versus time, we can observe a clear correlation for thin targets with circular polarization [Figs. 4(e) and 4(f)]. Here we use a Gaussian rather than a super-Gaussian focus, and so the curvature is across the entire focal spot rather than simply at the edges of the focus. These hot electrons form a sheath field, which is strongest near the focal area. 168 fs after the pulse interacts, TNSA has accelerated protons to appreciable energies (10–20 MeV) for the thin targets, with the focal area protons possessing not only higher energies but also a much larger divergence [Figs. 4(a) and 4(c)]. The increased divergence of the focal area protons is predominantly due to the initial curvature of the target and the subsequent acceleration from sheath fields. For both polarizations the proton energy spectra was exponential for the TNSA accelerated protons. A much smaller population with a large divergence due to RPA indicated a narrow energy spread peak between 30 and 60 MeV.

Thicker targets take longer to accelerate the focal volume and as a result will deform at much later times. Hence, for circular polarization significantly less energy can be absorbed into hot electrons. The maximum proton energy decreases slightly for TNSA accelerated protons in the linear case compared with thin targets, whereas for circular polarization acceleration is almost entirely suppressed.

In the 2D simulations, protons in the focal area display a divergence of $\sim\pi$ radians. Using this to estimate the solid angle emission of 2π steradians, for a proton density of 10^{23} cm^{-3} and our detector solid angle, we would expect only on the order of $\sim$1 protons to enter our detector. By contrast, protons from the surrounding area that undergo TNSA have a much smaller divergence, on the order of milliradians. We can estimate $\sim 10^6$ protons can reach the detector, a difference in 6 orders of magnitude, which explains the absence of RPA protons in the experimental measurement.

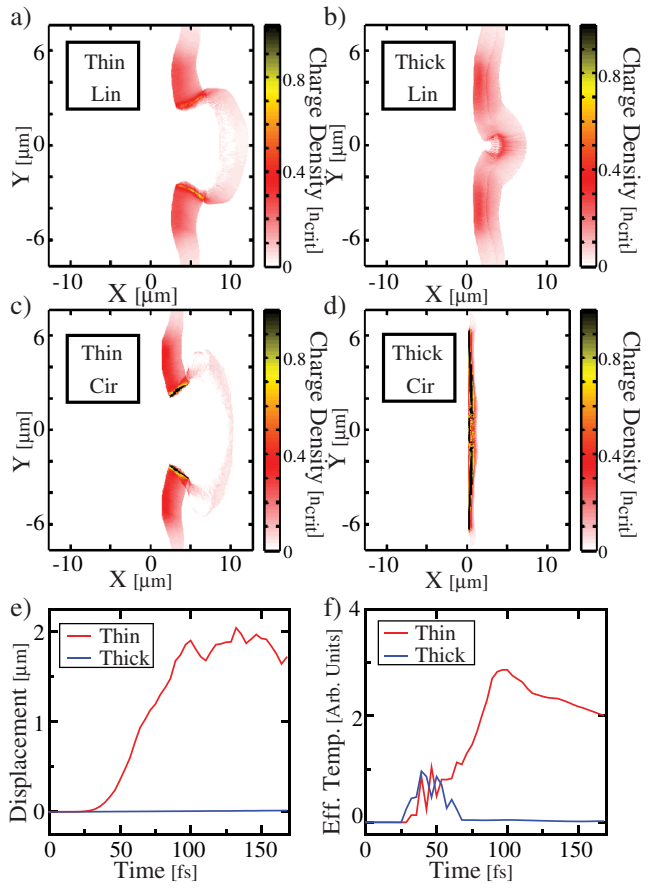

FIG. 4 (color online). Proton density space of OSIRIS 2D particle-in-cell simulations for (a) thin linear, (b) thick linear, (c) thin circular, and (d) thick circular cases taken at 168 fs. For the circular case, the mean target displacement along the laser axis v time is shown in (e), and the effective temperature v time is shown in (f). "Thin" and "thick" correspond to a total target thickness of 36 and 108 nm, respectively, with the target left justified at an x position of 0.

However, a narrow energy spread feature in the spectra is observed for thin foil C_6^+ ions, which are likely to be RPA ions from the focal area. The TP has a much higher sensitivity to carbon ions, allowing them to be distinguished from the background [Figs. 3(a) and 3(b)]. The simulations suggest that the focal volume ions on the rear of the target gain some velocity from the initial RPA interaction but lose desirable beam qualities due to the subsequent acceleration by the sheath.

It is evident then that the experimental conditions are not matched to the RPA regime due to the finite spot effects. The focal spot used in our studies is Gaussian, which will exhibit deformation effects throughout the focus rather than the "difficult to make" flattop focus. Femtosecond shaping of the pulse after plasma mirrors would also be very difficult. It is impractical to simply increase the spot size to increase total flux, as increasing the focal diameter increases the required power quadratically, meaning that an increase in focal diameter to even a 5 μm spot size would increase the required power to 2.5 petawatts, beyond current laser capabilities. Mass limited targets may suppress the effects of electron heating, but for thin foils these would be difficult to fabricate. Decreasing intensity would require more laser energy to achieve effective acceleration.

In conclusion, we have performed experiments investigating the effects of circular polarization on ion acceleration with ultrashort pulses at high intensity. We find that, below a threshold thickness of 100 nm, circular polarization begins to heat electrons and accelerate the surrounding contaminant ions via TNSA. Simulations show that target deformation provides a mechanism for laser energy to efficiently couple to the electrons, and TNSA occurs as a result. To minimize electron heating and more efficiently transfer momentum to the target, one would likely require comparable intensities but with a much larger focal diameter, requiring laser energies beyond current capabilities, which may be possible on future platforms [25].

This work was supported by the National Science Foundation through the Physics Frontier Center FOCUS (Grant No. PHY-0114336) and Graduate Research Fellowship Program (Grant No. DGE-0718128), as well as from the Office of Naval Research. We acknowledge the OSIRIS consortium (UCLA/IST Portugal) for the use of OSIRIS. Simulations were performed on the Nyx Cluster at University of Michigan.

[1] S. V. Bulanov, T. Zh. Esirkepov, V. S. Khoroshkov, A. V. Kuznetsov, and F. Pegoraro, Phys. Lett. A **299**, 240 (2002).
[2] E. Fourkal, B. Shahine, M. Ding, J. S. Li, C.-M. Ma, and T. Tajima, Med. Phys. **29**, 2788 (2002).
[3] G. Petrov and J. Davis, Phys. Plasmas **18**, 073102 (2011).
[4] V. Malka *et al.*, Med. Phys. **31**, 1587 (2004).
[5] E. L. Clark *et al.*, Phys. Rev. Lett. **84**, 670 (2000); A. Maksimchuk, S. Gu, K. Flippo, D. Umstadter, and V. Yu. Bychenkov, *ibid.* **84**, 4108 (2000); R. A. Snavely *et al.*, *ibid.* **85**, 2945 (2000); S. C. Wilks, A. B. Langdon, T. E. Cowan, M. Roth, M. Singh, S. Hatchett, M. H. Key, D. Pennington, A. MacKinnon, and R. A. Snavely, Phys. Plasmas **8**, 542 (2001).
[6] S. P. Hatchett *et al.*, Phys. Plasmas **7**, 2076 (2000).
[7] T. Toncian *et al.*, Science **312**, 410 (2006).
[8] B. M. Hegelich, B. J. Albright, J. Cobble, K. Flippo, S. Letzring, M. Paffett, H. Ruhl, J. Schreiber, R. K. Schulze, and J. C. Fernández, Nature (London) **439**, 441 (2006); H. Schwoerer, S. Pfotenhauer, O. Jäckel, K.-U. Amthor, B. Liesfeld, W. Ziegler, R. Sauerbrey, K. W. D. Ledingham, and T. Esirkepov, Nature (London) **439**, 445 (2006).
[9] F. Dollar *et al.*, Phys. Rev. Lett. **107**, 065003 (2011).
[10] D. Jung *et al.*, Phys. Rev. Lett. **107**, 115002 (2011).
[11] L. Yin, B. J. Albright, B. M. Hegelich, and J. C. Fernández, Laser Part. Beams **24**, 291 (2006).
[12] S. S. Bulanov *et al.*, Phys. Rev. E **78**, 026412 (2008).
[13] A. P. L. Robinson, M. Zepf, S. Kar, R. G. Evans, and C. Bellei, New J. Phys. **10**, 013021 (2008).

[14] C. Palmer *et al.*, Phys. Rev. Lett. **106**, 014801 (2011).
[15] A. Henig *et al.*, Phys. Rev. Lett. **103**, 245003 (2009).
[16] T. Esirkepov, M. Borghesi, S. V. Bulanov, G. Mourou, and T. Tajima, Phys. Rev. Lett. **92**, 175003 (2004).
[17] X. Yan, C. Lin, Z. M. Sheng, Z. Y. Guo, B. C. Liu, Y. R. Lu, J. X. Fang, and J. E. Chen, Phys. Rev. Lett. **100**, 135003 (2008).
[18] A. Macchi, S. Veghini, T. V. Liseykina, and F. Pegoraro, New J. Phys. **12**, 045013 (2010).
[19] V. Chvykov, P. Rousseau, S. Reed, G. Kalinchenko, and V. Yanovsky, Opt. Lett. **31**, 1456 (2006).
[20] W. Mróz *et al.*, Rev. Sci. Instrum. **67**, 1272 (1996).
[21] M. C. Kaluza, J. Schreiber, M. I. K. Santala, G. D. Tsakiris, K. Eidmann, J. Meyer-ter-Vehn, and K. J. Witte, Phys. Rev. Lett. **93**, 045003 (2004).
[22] R. O. Fonseca *et al.*, Lect. Notes Comput. Sci. **2331**, 342 (2002).
[23] C. Gahn, G. D. Tsakiris, A. Pukhov, J. Meyer-ter-Vehn, G. Pretzler, P. Thirolf, D. Habs, and K. J. Witte, Phys. Rev. Lett. **83**, 4772 (1999).
[24] F. Brunel, Phys. Rev. Lett. **59**, 52 (1987).
[25] G. Mourou and T. Tajima, Opt. Photonics News **22**, 47 (2011).